The Astrophysical Journal, 886:132 (12pp), 2019 December 1 https://doi.org/10.3847/1538-4357/ab4a17

Waldmeier Effect in Stellar Cycles

Suyog Garg[1], Bidya Binay Karak[2], Ricky Egeland[3], Willie Soon[4], and Sallie Baliunas[4,5]
[1] Indian Institute of Information Technology, Design and Manufacturing, Kancheepuram, Chennai 600127, India
[2] Department of Physics, Indian Institute of Technology (Banaras Hindu University), Varanasi 221005, India
[3] High Altitude Observatory, National Center for Atmospheric Research, 3080 Center Green Dr., Boulder, CO 80301, USA
[4] Harvard-Smithsonian Center for Astrophysics, Cambridge, MA 02138, USA
Received 2019 August 14; revised 2019 September 25; accepted 2019 September 30; published 2019 November 29

Abstract

One of the most robust features of the solar magnetic cycle is that the stronger cycles rise faster than the weaker ones. This is popularly known as the Waldmeier Effect, which has been known for more than 100 yr. This fundamental feature of the solar cycle has not only practical implications, e.g., in predicting the solar cycle, but also implications in understanding the solar dynamo. Here we ask whether the Waldmeier Effect exists in other Sun-like stars. To answer this question, we analyze the Ca II H and K *S*-index from Mount Wilson Observatory for 21 Sun-like G–K stars. We specifically check two aspects of Waldmeier Effect, namely, (1) WE1: the anticorrelation between the rise times and the peaks and (2) WE2: the positive correlation between rise rates and amplitudes. We show that, except for HD 16160, HD 81809, HD 155886, and HD 161239, all stars considered in the analysis show WE2, while WE1 is found to be present only in some of the stars studied. Furthermore, the WE1 correlation is weaker than the WE2. Both WE1 and WE2 exist in the solar *S*-index as well. Similar to the solar cycles, the magnetic cycles of many stars are asymmetric about their maxima. The existence of the Waldmeier Effect and asymmetric cycles in Sun-like stars suggests that the dynamo mechanism which operates in the Sun is also operating in other stars.

Unified Astronomy Thesaurus concepts: Solar cycle (1487); Stellar activity (1580); Solar magnetic fields (1503); Solar dynamo (2001); Stellar types (1634)

1. Introduction

The solar magnetic activity increases and decreases cyclically with an average period of 11 yr; however, both the duration and amplitude vary cycle to cycle. There are also short-term variations within the cycle (Lean & Brueckner 1989), making it difficult to predict future activity. Nonetheless, there are some special features of the solar cycle. One of these is that the rate of increase of the activity is not the same for all cycles, rather it depends on the strength of the cycle. This leads to a famous relation, now widely known as the Waldmeier Effect (Waldmeier 1935), though it was in fact been noticed earlier (Halm 1901, 1902). It says that the stronger cycles rise faster (and take less time to reach their peak activities) than the weaker ones, and vice versa. The Waldmeier Effect has been extensively studied in different proxies of solar activity data since its discovery in 1935. However, limitations on different data sets sometimes make it difficult to establish its existence. For example, Dikpati et al. (2008) did not find a significant anticorrelation between rise times and amplitudes and claimed that the Waldmeier Effect is not present in the sunspot area data. Later, a more careful analysis by Karak & Choudhuri (2011) computed the rise time and showed that the Waldmeier Effect exists in all sunspot area, number, and 10.7 cm radio flux data. They further showed that this anticorrelation between rise times and amplitudes is one aspect of the Waldmeier Effect that they referred to as WE1. The other aspect is the positive correlation between the rise rates and the amplitudes and they referred to it as WE2. It turned out that the latter feature is much more robust and probably more useful (Cameron & Schüssler 2008). For example, when the Waldmeier Effect is used to predict the future solar cycle, WE2 is meant rather than WE1 which requires rise time of the cycle (e.g., Cameron & Schüssler 2007; Kane 2008; Ramesh & Lakshmi 2012). Only after the cycle has reached its maximum can the rise time be obtained while the rise rate can easily be obtained shortly after the cycle has started.

Many other stars, so-called the Sun-like stars (with spectral types F–M), which have convection zones in their outer layers produce magnetic fields through dynamo action (Parker 1955; Moffatt 1978; Gilman 1983; Noyes et al. 1984; Soon et al. 1993; Saar & Brandenburg 1999; Ossendrijver 2003; Charbonneau 2014). Many of these stars indeed show clear magnetic cycles with varying amplitudes and durations (Baliunas et al. 1995). Therefore, the important question that we want to answer in this paper is whether the Waldmeier Effect can be seen in other stars as well. Checking the Waldmeier Effect in other stars, however, is challenging because typically we do not have a long data set of magnetic activity. Among the available observables of magnetic activity, Ca II H and K line emission (hereafter simply HK) is the longest data set that has been used to study the long-term variation of stellar activity. The magnetic (nonthermal) heating in the chromosphere causes emission in the cores of HK. This HK emission is used to measure the stellar magnetic activity due to its strong correlation with the magnetic flux, as realized in the Sun (Leighton 1959; Skumanich et al. 1975; Schrijver et al. 1992).

The HK Project of Mount Wilson Observatory (MWO) regularly monitored more than 100 Sun-like stars with spectral types early F to M, starting from 1966. However, the project ended in 2003. Therefore, this limited data of 37 yr may be used to analyze the features of stellar cycles. Analyzing these data from 21 stars for which good cycles are seen, we shall explore the existence of the Waldmeier Effect in different Sun-like stars for the first time. Other features of stellar cycles, particularly the

[5] Retired.

asymmetry of the cycles will also be identified. To put the Sun in this context, we shall also present the analysis of the Waldmeier Effect using the same Ca II HK proxy obtained from the Kodaikanal Observatory, which was not done in the past.

2. Data Analyses

We use the fully calibrated *S*-index time series from the MWO HK Project. In our analysis we need high-quality data with at least two consecutive unambiguous cycles. These are available only in G and K stars which are also listed in Böhm-Vitense (2007) and Schröder et al. (2013). From these lists, we find that only 21 stars are useful in our study. Chromospheric variations of these stars are shown in Figure 1, while the cycle properties are listed in Table 1. The dotted points in this figure show the raw data, the calibrated *S*-index. The *S*-index for the Sun, obtained from the Kodaikanal Observatory is also shown for comparison in Figure 2.

To study the Waldmeier Effect using these *S*-index data, we need to compute the rise time, rise rate, and peak value of each cycle. However, as can be seen from Figure 1, the data are irregular (due to the rotation, active region emergence, and decay, as well as uneven observations). Thus, we end up getting huge uncertainties in the cycle parameters if they are computed directly from the calibrated *S*-index. Therefore, instead of using the raw calibrated *S*-index data, we produce approximate cycles of the data using the given profile(s) and then we use the best-fitted cycles to study the Waldmeier Effect. What profile we use to produce the fitted data is guided by the fitting of solar data. A popular fitting profile of the solar cycle is the following quasi-Planck function (Hathaway et al. 1994)

$$f(t) = \frac{a(t - t_0)^3}{\exp\left[\frac{(t-t_0)^2}{b^2}\right] - c}, \tag{1}$$

where t is the time in year, t_0 is the starting time of the cycle, parameters a, b, and c are related to the cycle amplitude (peak *S*-index), the rise time, and the cycle asymmetry, respectively. On the other hand, Du (2011) has demonstrated that the following skewed-Gaussian function captures the solar cycle profile slightly better.

$$f(t) = A \exp\left[\frac{-(t - t_m)^2}{2B^2[1 + \alpha(t - t_m)]^2}\right] + f_{\min}, \tag{2}$$

where A is related to the cycle amplitude, $t_{\rm m}$ is approximately the time of maximum, B relates to the width of the cycle rising phase, and α is the asymmetry parameter. The last term $f_{\min}$, which measures the offset *S*-index at the cycle minimum, was not present in the Du (2011) model, but was introduced recently by Egeland et al. (2017). Although they preferred this profile, they have shown that the fitting with the quasi-Planck function produces comparable results. We, therefore, fit the stellar *S*-index with both profiles and study the Waldmeier Effect separately in each fitted data.

As the fitting will be performed for each cycle separately, we need to isolate the cycles first. To do so, we bin the raw data with one-year intervals and then smooth with a three-point running window. In this smoothed *S*-index, the cycles are isolated by considering the data in between two successive minima. The individual cycle periods computed from two successive minima and their mean periods for all stars are enlisted in the last two columns of Table 1. Taking the minimum time as a heuristic value, we proceed to fit the raw *S*-index of individual cycles with functions given in Equations (1) and (2). For the fitting, we use the Python `scipy` library `curve_fit` routine. This built-in function uses a Trusted Region Reflective method with the Levenberg–Marquardt algorithm applied to trusted-region subproblems (Moré 1978, p. 105). In Figures 1 and 2, the solid and dashed lines show the fitted profiles using skewed-Gaussian (Equation (2)) and quasi-Planck functions (Equation (1)), respectively. To measure a goodness of fit we compute the reduced $\chi^2_{\rm red}$. In evaluating $\chi^2_{\rm red}$, we consider the error as 1.2% of the *S*-index as suggested in Baliunas et al. (1995). Tables 3 and 4 in the Appendix list the values of various fitted parameters and $\chi^2_{\rm red}$ for each of the stars used in the analysis. While for most stars these $\chi^2_{\rm red}$ values are reasonable considering that the models do not address short-timescale variability present in the data, we get significantly large values for a few stars where even the long-term variability appears to be not well represented by the models. We further observe that the c column for quasi-Planck fit contains some extreme negative values. As such, although the trend is seen in general for most of the stellar cycles, it cannot be said that the parameter c corresponds to the cycle asymmetry. It can also be seen that the parameter t_0 does not increase monotonically in every consecutive cycle of a star. Thus, the correspondence between t_0 and the cycle start time is also not thorough.

Sadly, not all the cycles are usable for the analysis. The observational data of most of the stars contains a partial cycle either initially or at the end of the observation period. These partial cycles cannot be used. Further, some cycles of HD 155885, HD 155886, and HD 201092 are unusable because of ill-fitting or inconsistent variability. The Appendix contains tables detailing the fit parameter values for all the stars. Table 3 of the Appendix lists the parameter values for the usable cycles, whereas Table 4 gives the values for the unusable cycles. The plots in Figure 1 can be reproduced from Equations (1) and (2) using the parameters given in Tables 3 and 4. To compare the goodness of the fitting of different stars we further compute $\chi^2_{\rm red}$ for all the usable cycles in each star. This total $\chi^2_{\rm red}$ is shown in Table 1. For the solar cycles, we get $\chi^2_{\rm red}$ values as 3.5 for quasi-Planck and 2.5 for skewed-Gaussian fittings.

We note that the observational data of the stellar magnetic activity sometimes contains local minima between the cycles. We ignore the local minima when the time difference between the minimum and the preceding maximum is much less compared to such difference for other cycles. The threshold value of the time difference for this criterion of ignoring the local minima varies from star to star and depends on the cycle characteristics. For instance, for HD 201092, the local minima are ignored if the time interval containing the minimum is ∼3 yr or less. Whereas, in the case of HD 149661, since the actual cycle durations are in that range, we do the same for a much smaller interval (∼1 yr).

Furthermore, another important parameter to look into is the cycle asymmetry. Solar magnetic cycles are usually found to be asymmetric about the maxima. Therefore it is interesting to find out whether the stellar cycles are also asymmetric. A measure of this asymmetry in the cycle can be obtained by calculating the skewness of the data defined as

$$\gamma_1 = \frac{\sum_{i=1}^{N}(f_i^d - \bar{f})^3}{(N - 1)\,\sigma_{\rm fit}^3}, \tag{3}$$

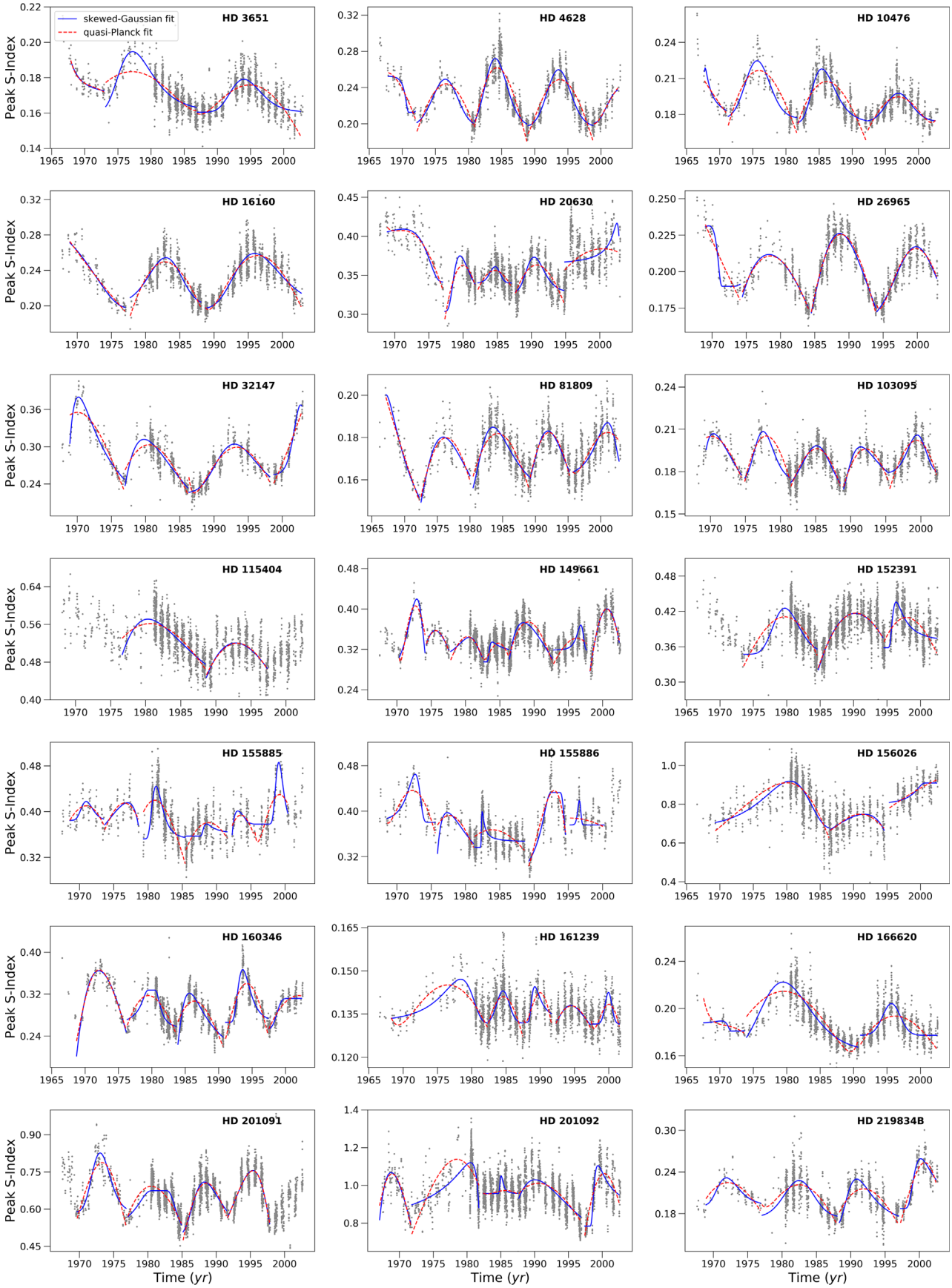

Figure 1. Stellar cycles used in our analysis. Dotted points are the MWO's calibrated *S*-index, while solid blue and dashed red lines are the fitted data using skewed-Gaussian and quasi-Planck functions, respectively.

Table 1
Summary of Data Analysis and Results

Star	SpecType	Data Duration	# Cycles	$\chi^2_{\rm red,P}$	$\chi^2_{\rm red,G}$	$\overline{\gamma_1}$	WE1?	WE2?	$P_{\rm cyc}$ (yr)	$P_{\rm cyc}^{\rm mean}$ (yr)
HD 3651	K0V	1966–2002	2	12.6	11.0	2.26	WE1$^{\rm G}$	WE2$^{\rm G}$	13.81, 15.99	14.90
HD 4628	K2V	1966–2002	3	20.5	11.6	0.60	WE1$^{\rm P,G}$	WE2$^{\rm P,G}$	8.67, 8.08, 9.98	8.91
HD 10476	K1V	1966–2002	3	16.5	10.7	0.85	No	WE2$^{\rm P,G}$	10.50, 10.57, 10.61	10.56
HD 16160	K3V	1967–2002	2	18.6	17.8	0.00	WE1$^{\rm G}$	No	10.99, 14.31	12.65
HD 20630	G5V	1967–2002	3	11.0	9.5	0.10	WE1$^{\rm G}$	WE2$^{\rm P,G}$	4.83, 5.50, 7.21	5.85
HD 26965	K1V	1967–2002	3	8.9	8.8	0.02	No	WE2$^{\rm P,G}$	10.08, 9.58, 8.96	9.54
HD 32147	K3+V	1967–2002	2	21.2	19.2	0.08	WE1$^{\rm P,G}$	WE2$^{\rm P,G}$	9.33, 12.42	10.88
HD 81809[a]	G2IV+G2V	1966–2002	4	9.8	8.4	0.14	No	No	7.96, 8.74, 6.50, 7.32	7.64
HD 103095	KV	1968–2002	4	9.1	8.2	0.50	No	WE2$^{\rm P,G}$	6.58, 7.50, 6.58, 6.90	6.89
HD 115404	K2.5V	1968–2002	2	25.8	25.4	−0.19	WE1$^{\rm P,G}$	WE2$^{\rm G}$	11.99, 8.84	10.42
HD 149661	K0V	1967–2002	7	23.0	20.6	0.34	No	WE2$^{\rm P,G}$	3.95, 3.54, 4.84, 3.75, 6.42, 5.34, 4.46	4.61
HD 152391	K8+V	1966–2002	3	28.7	24.6	−0.15	WE1$^{\rm G}$	WE2$^{\rm P,G}$	11.16, 9.83, 8.10	9.70
HD 155885	K1V	1967–2002	4	29.3	19.7	0.30	No	WE2$^{\rm P}$	5.08, 5.67, 6.19, 1.47	4.60
HD 155886	K2V	1967–2002	2	25.4	23.7	0.30	WE1$^{\rm P}$	No	7.33, 5.99	6.67
HD 156026	K5V	1966–2002	2	75.3	74.1	−0.58	No	WE2$^{\rm P}$	17.16, 8.87	13.02
HD 160346	K2.5V	1966–2002	4	28.2	16.4	0.22	No	WE2$^{\rm P,G}$	7.58, 7.58, 7.13, 6.45	7.19
HD 161239	G2IIIb	1966–2001	5	8.0	7.6	0.55	No	No	14.17, 5.17, 4.67, 5.17, 4.29	6.69
HD 166620	K2V	1966–2002	2	22.4	17.4	5.99	WE1$^{\rm P,G}$	WE2$^{\rm G}$	17.08, 11.59	14.34
HD 201091	K5V	1967–2002	4	27.7	28.5	0.39	No	WE2$^{\rm P,G}$	7.42, 8.08, 6.50, 6.52	7.13
HD 201092	K7V	1967–2002	3	56.9	39.6	−0.07	No	WE2$^{\rm P}$	4.76, 10.58, 5.32	6.89
HD 219834B	K2V	1967–2002	4	50.5	38.0	0.36	WE1$^{\rm G}$	WE2$^{\rm P,G}$	8.10, 11.25, 8.92, 5.47	8.45
Sun	G2V	1913–2016	10	3.5	2.5	0.34	WE1$^{\rm P,G}$	WE2$^{\rm P,G}$	7.84–11.49	10.35

Note. Here, "# cycles" is the total number of usable cycles present in the data duration. $\chi^2_{\rm red,P}$ and $\chi^2_{\rm red,G}$ are the reduced χ^2 computed over all usable cycles of a star fitted with quasi-Planck (Equation (1)) and skewed-Gaussian (Equation (2)) profiles, respectively. $\overline{\gamma_1}$ is the mean Skewness γ_1 (a measure of the cycle asymmetry) for the usable cycles. Furthermore, the superscripts on the WE1 and WE2 tell the fitting in which the correlation is found. Here, P stands for quasi-Planck fit, while G stands for skewed-Gaussian. The spectral type information is taken from Oláh et al. (2016).
[a] HD 81809 is an unresolved binary and the observed activity cycles are most likely linked to a G2 subgiant (Egeland 2018).

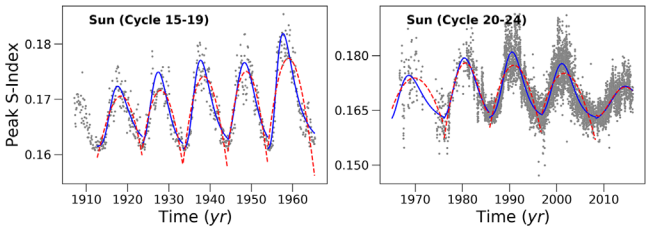

Figure 2. Same as Figure 1 but for the Sun. (Left) Kodaikanal Observatory data and (right) MWO data scaled; see Egeland et al. (2017) for details.

where $\bar{f}$ is the mean strength of the cycle and $\sigma_{\rm fit}$ is the standard deviation of the cycle data from the fitted profile. Column 7 of Table 1 tabulates the mean value of the skewness for the stars $\overline{\gamma_1}$, calculated using the individual skewness values of usable cycles. A positive (negative) skewness means that the part of the cycle on the right (left) of the cycle maxima is skewed compared to the other side. For reference, the mean skewness of the solar cycles computed from our *S*-index is 0.3373.

3. Results

3.1. Checking the Waldmeier Effect in Solar S-index

As mentioned in the Introduction, previous authors have studied the Waldmeier Effect using sunspot number and area data, but not using any chromospheric magnetic proxy. Therefore, we shall first check the Waldmeier Effect for the Sun with the same type of chromospheric magnetic proxy that we are using for the other stars. This will show the robustness of our analysis and also put the Sun in the stellar context. For this, we use the *S*-index of Sun from MWO data for the last 5 cycles and Kodaikanal data where the data is available for cycles 15–19. As described in Egeland et al. (2017), these two data sets are made homogeneous by doing the following scaling.

The Kodaikanal data is in Integrated Sunlight Spectrometer (ISS) flux scale, calibrated by Bertello et al. (2016) using the synoptic Ca II *K* plage index from spectroheliograms from the Kodaikanal (KKL) Observatory in India. This time series data of Ca II *K* emission is first transformed to the Ca II H and K measurement scale of Sacramento Peak National Observatory (NSO/SP) flux scale by applying the following equation

$$K_{\rm KKL(SP)} = 1.1388 K_{\rm KKL(ISS)} - 0.0071. \quad (4)$$

Now, another transformation is performed between the NSO/SP *K* emission index and the MWO *S*-index. Assuming a linear relationship of the form, $S(K) = a + bK$, and using the cycle 23 fit parameters for the Sun (Egeland et al. 2017), the following linear transformation is obtained:

$$S(K) = (1.5 \pm 0.13)K + (0.031 \pm 0.013). \quad (5)$$

Using Equation (5) for the Kodaikanal data between cycles 15–19, homogenizes the solar data.

Previous studies have shown that the WE2 (anticorrelation between rise rates and amplitudes) is a robust feature of the solar cycle. Therefore, we analyze the WE2 first using the data obtained from the quasi-Planck fitting. Following Karak & Choudhuri (2011), we define the rise rate of a cycle as the

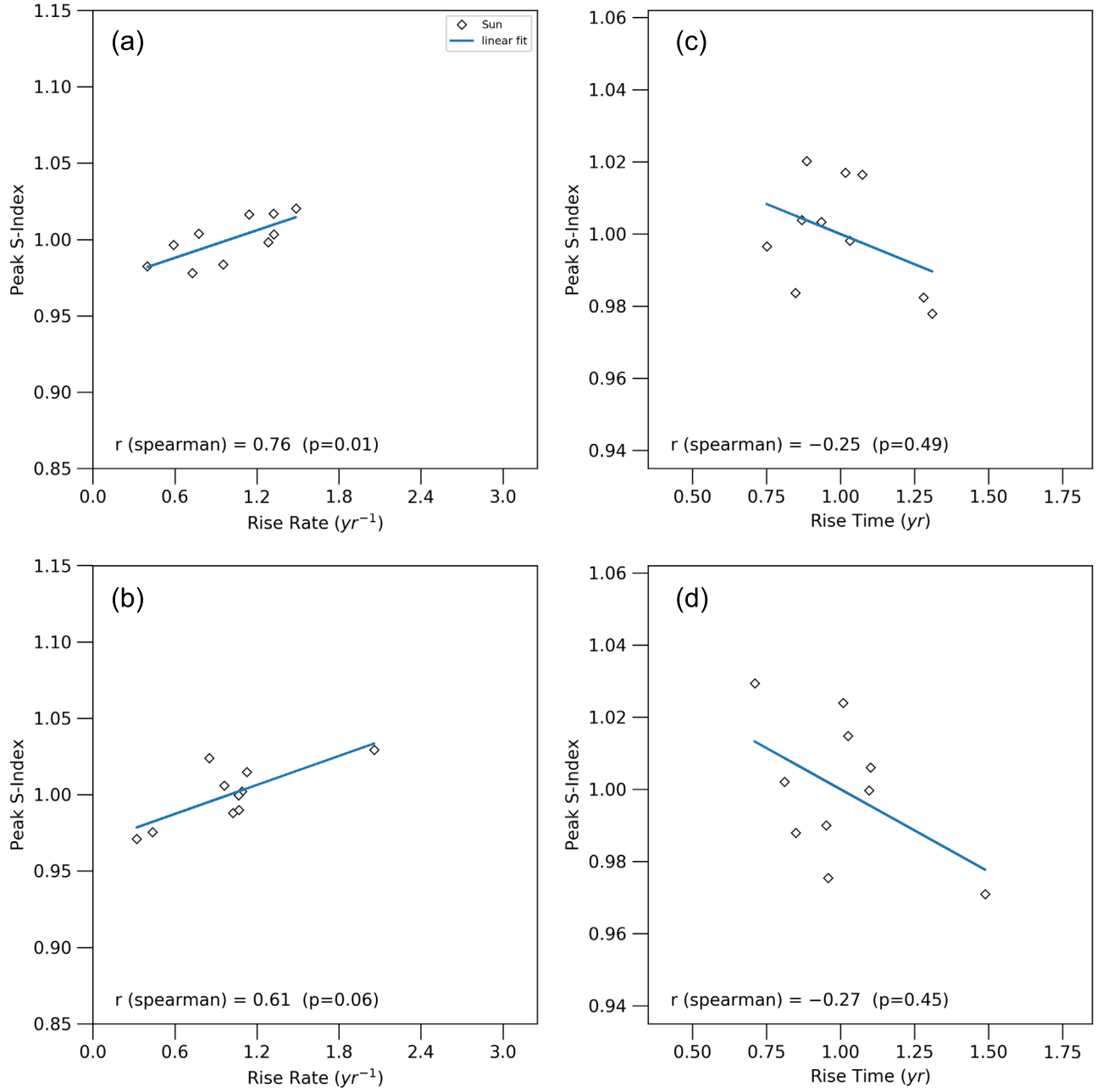

Figure 3. Left: scatter plots for WE2 (positive correlation between rise rates and the amplitudes). Right: WE1 (anticorrelation between rise times and amplitudes) for the solar cycles. Top and bottom panels obtained from quasi-Planck and skewed-Gaussian fitted data, respectively. The solid lines are linear fits with slopes $m = 0.030 \pm 0.023$, 0.032 ± 0.022, -0.033 ± 0.062, and -0.045 ± 0.064 and intercepts $c = 0.970 \pm 0.025$, 0.968 ± 0.024, 1.033 ± 0.063, and 1.046 ± 0.065, with the rms deviation of fittings being 0.011, 0.013, 0.014, and 0.018, respectively, for panels (a)–(d).

change in the activity in a single year and calculating the change between two consecutive years after leaving out one year from the cycle beginning (minimum). The scatter plot between the rise rate and the peak *S*-index is shown in the left panel of Figure 3 both for the quasi-Planck and skewed-Gaussian fittings. We find that the correlation is good and the value of the correlation coefficient is comparable to the previous study (Cameron & Schüssler 2008; Karak & Choudhuri 2011).

Now, we consider WE1 which is the anticorrelation between the rise time and the strength. As argued in Dikpati et al. (2008) and Karak & Choudhuri (2011), incorrect identification of cycle minimum or maximum can lead to a large error in the rise time computed. We therefore consider the rise time as the time taken by a cycle to grow from 20% to 80% of its peak. The scatter plot between the rise time and the peak *S*-index is shown in the right panel of Figure 3. As found in the other proxies of the solar cycle, the WE1 correlation is much weaker. The correlation coefficients found in our *S*-index data is comparable to the previous values obtained from other proxies of the solar data (Dikpati et al. 2008; Karak & Choudhuri 2011).

3.2. Checking the Waldmeier Effect in Stars

Now we study the Waldmeier Effect for the stars in the same way as we have done for the Sun. We first show the results of WE2 using the data obtained from the quasi-Planck fitting. For the representation, the scatter plots between the rise rates and

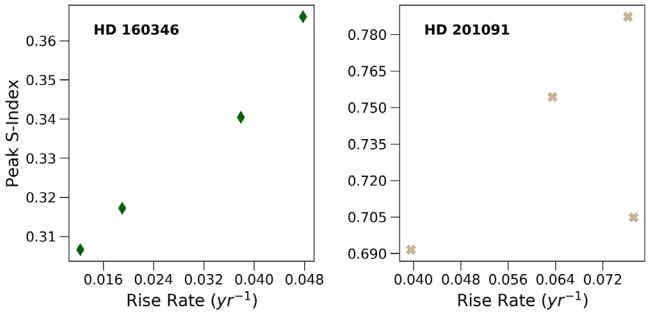

Figure 4. WE2 obtained from the quasi-Planck fitted *S*-index data of stars HD 160346 (left) and HD 201091 (right).

the peak *S*-indexes for HD 160346 and HD 201091 are shown in Figure 4. This shows that the stronger cycles rise faster than the weaker ones—establishing the WE2 in these two stars. As the number of cycles in each star is very limited, the correlation coefficient computed from the cycles of an individual star is not very meaningful. Therefore, we combine the data for all the stars that individually show the correlation for WE2. For a star, if the Spearman correlation coefficient between rise rates and amplitudes is at least 0.1, then we mark that star to "hold WE2." This information is listed in Table 1. Table 5 in the Appendix details the peak *S*-index and rise rate values for all the stars used in the analysis. Surprisingly, we find that all the stars except HD 16160, HD 81809, HD 155886, and HD 161239, follow WE2 for at least one type of fitting.

For HD 16160, there are only two cycles (see Figure 1). Therefore, with this limited data, it is difficult to make a conclusive comment about whether HD 16160 truly does not follow WE2. The same argument may hold for HD 155886 because this star also has only two usable cycles and both cycles are very noisy. In HD 161239, the correlation is destroyed due to the first cycle which is very different from the rest. As seen in Figure 1, for HD 161239, the first cycle is the strongest one and the activity level during the minimum is relatively high. This produces an unexpectedly slow rise rate in the first cycle and breaks the WE2 relation. If we do not consider the first cycle, then the star beautifully shows WE2. (The linear Spearman correlation is 0.80 for quasi-Planck fitted data and 0.20 for skewed-Gaussian fitting.) In the case of HD 81809, the cycles are very regular and the data quality is good. However, it is very surprising that the star does not follow WE2. The individual Spearman correlation coefficient between the rise rates and the amplitudes is −0.80 for the quasi-Planck fitting and −0.40 for the skewed-Gaussian. Thus the correlation is opposite to the one we expect for the WE2 to hold.

The combined data of stars having a good positive correlation between the rise rate and the amplitude are shown in the top panel of Figure 5. We note that different stars have different activity levels and cycle growth rates. Thus, to put all values in a comparable range, we normalize the data of individual stars with their average values. This does not affect the value of the correlation coefficient of the combined data. For comparison, the data from the Sun is also shown in the same plot. As seen from the top panel of Figure 5, the composite data show a good correlation between rise rates and strengths, excluding the solar data and with the linear Spearman correlation coefficient being 0.72. The data obtained from the skewed-Gaussian fitting show a similar behavior, although the correlation coefficient is lower; see the bottom

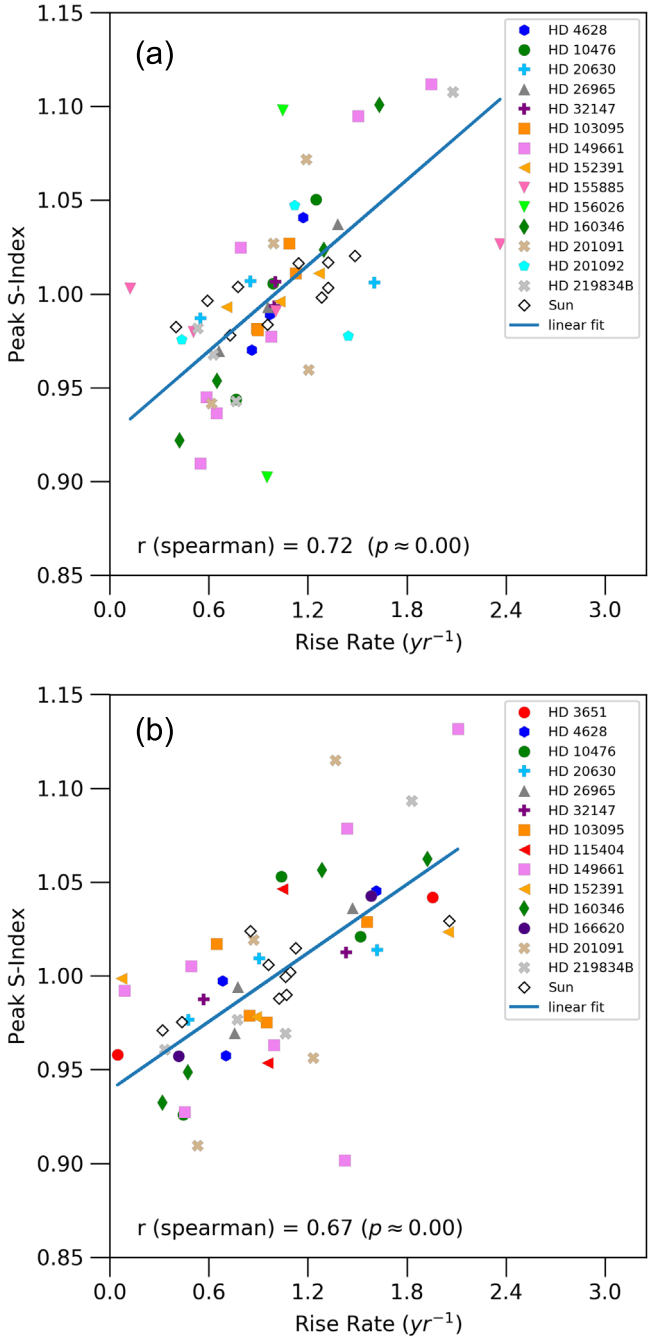

Figure 5. Combined scatter plot for WE2. Different symbols represent different stars. The linear Spearman correlation and confidence level are printed on each plot. Top and bottom panels obtained from quasi-Planck and skewed-Gaussian fitted data. We note that the data of stars HD 16160, HD 81809, HD 155886, and HD 161239 are not included because these stars do not show a positive correlation. The solid lines are best linear fits with slopes $m = 0.076 \pm 0.025$ and 0.061 ± 0.021 and intercepts $c = 0.924 \pm 0.028$ and 0.939 ± 0.024, with the rms deviation of fittings being 0.038 and 0.039, respectively, for top and bottom panels.

panel of Figure 5. Interestingly, the skewed-Gaussian profile fits the data better than the quasi-Planck profile (less $\chi^2_{\rm red,G}$ values as seen from Table 1); however, the Waldmeier relation is relatively weaker.

Finally, we explore WE1 for stars. Again, we first check the trend between rise times and the peaks for each star separately. We say that a star shows WE1 if the Spearman correlation

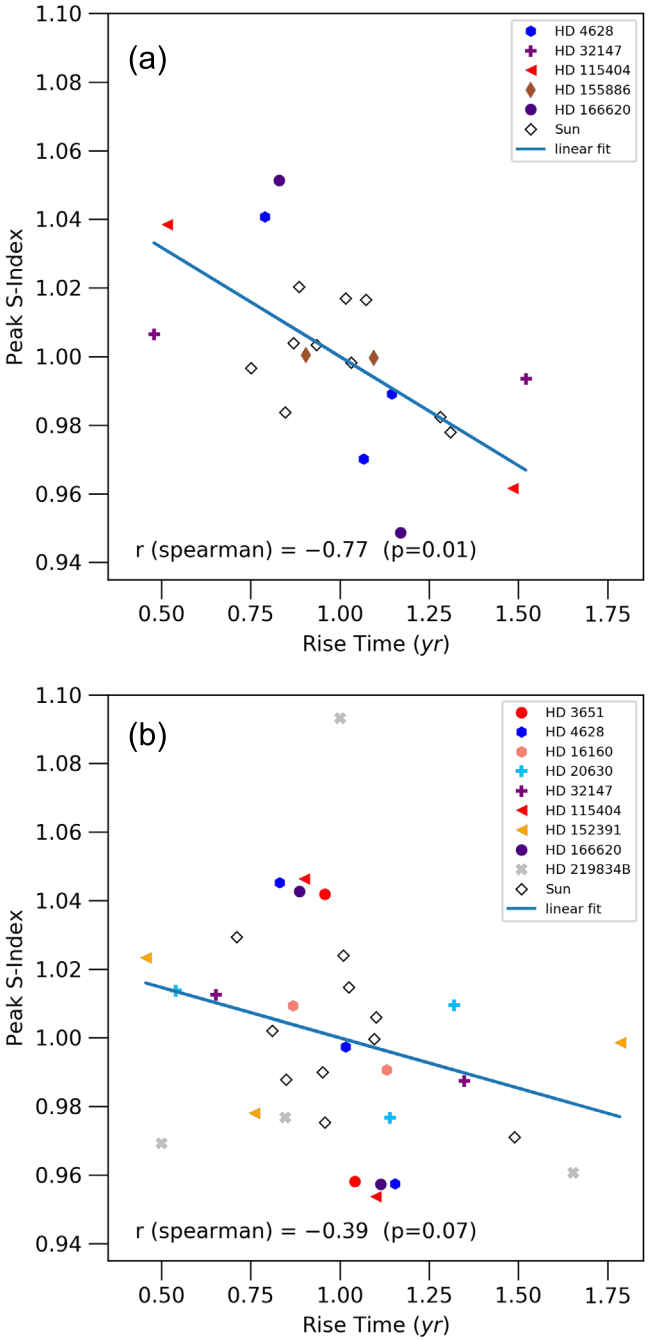

Figure 6. Scatter plot for WE1. The figure format is the same as that of Figure 5; however, in this case the number of stars following solar-like WE1 is lower. The solid lines are linear fits with slopes $m = -0.064 \pm 0.055$ and -0.029 ± 0.049 and intercepts $c = 1.064 \pm 0.058$ and 1.029 ± 0.051, with the rms deviation of fittings being 0.026 and 0.036, respectively, for top and bottom panels.

coefficient between peaks and rise times is less than −0.1. As listed in Table 1, not all stars show the expected negative correlation. We find that only 5 stars out of 21 show WE1 for the quasi-Planck fitting. For the skewed-Gaussian fitting, four more stars show the solar-like WE1 correlation.

The scatter plots between rise times and peak *S*-index of all the stars showing WE1 individually are shown in Figure 6. The peak S-index and rise time values for all the stars are detailed in Table 5 of the Appendix. For comparison, the data for the Sun are overplotted in the same figure. In this figure, we observe

Table 2
WE1 Correlation Coefficients

t_{start}	t_{end}	$r_{Spearman}$	
		Quasi-Planck	Skewed-Gaussian
0.15	0.75	−0.80	−0.40
0.15	0.80	−0.81	−0.40
0.15	0.85	−0.78	−0.43
0.20	0.75	−0.80	−0.35
0.20	0.80	−0.77	−0.39
0.20	0.85	−0.75	−0.40
0.25	0.75	−0.82	−0.50
0.25	0.80	−0.81	−0.51
0.25	0.85	−0.81	−0.51

Note. t_{end} and t_{start} are the times at which the activity is the given fraction of the peak value. The rise time is defined as the time difference between the t_{end} and t_{start}. Stars used in the correlation computation are, for the quasi-Planck fitting case, HD 4628, HD 32147, HD 115404, HD 155886, and HD 166620, while for the skewed-Gaussian case, HD 3651, HD 4628, HD 16160, HD 20630, HD 32147, HD 115404, HD 152391, HD 166620, and HD 219834B.

that the correlation coefficient is much weaker. Excluding the solar data, the linear Spearman correlation coefficient is −0.77 ($p = 0.01$) for quasi-Planck fittings, while this value for skewed-Gaussian fitting is −0.39 ($p = 0.07$). Note that in the latter case, the correlation is much less and thus the results are statistically insignificant. It is the HD 219834B which has a very poor WE1 correlation (−0.02) and reduces the composite correlation in Figure 6(b). If we exclude this star, then the correlation becomes −0.52 ($p = 0.02$). Weaker correlation for WE1 is not surprising because it is already known from the study of solar data that WE1 is much weaker and it is sensitive to the data set in use as well as the computation of rise times (Dikpati et al. 2008; Karak & Choudhuri 2011). Fortunately, instead of defining rise time as the time taken by a cycle to grow from 20% to 80% of its peak, if we define it using different values, then we also get a solar-like negative correlation for WE1 from those stars which show correlations in Figure 6 (see Table 2). However, the correlation values for skewed-Gaussian remain far lower than those for the quasi-Planck fit.

Let us discuss a consequence of the WE2 relation. As shown in Figure 5, WE2 can be read as $S = m\left(\frac{dS}{dt}\right) + S_0$. Now if we make a crude assumption: $\frac{dS}{dt} = \frac{S}{t}$, where t is the total rise time, and if we also take the limit $\frac{m}{t} < 1$ (which is the case in our data), then to a first order, we find $S = (mS_0)\frac{1}{t} + S_0$. This relation fits the data presented in Figure 6 (WE1) poorly (rms deviation of the fittings being 0.029 and 0.037 for quasi-Planck and skewed-Gaussian fitted data). Our correlation plot for WE1 already has a large scatter and thus we cannot conclusively reject this variation over the linear variation represented as WE1.

4. Conclusion and Discussion

In this study, we for the first time have explored the Waldmeier Effect in Sun-like stars. We have used MWO's calibrated *S*-index of 21 stars having observations for at least two consecutive unambiguous cycles. These stars having high-quality cycles belong to the spectral index of G–K (three

G-stars and the rest are K-stars); see Egeland (2017) for the discussion on the cycle quality of MWO stars and Schröder et al. (2013) for an HR diagram of the cycling MWO stars. After carrying out systematic analyses of the data, we check two related aspects of the Waldmeier Effect, namely, WE1 (the anticorrelation between rise times and the amplitudes) and WE2 (the positive correlation between rise rates and amplitudes). We find that all these stars, except HD 16160, HD 81809, HD 155886, and HD 161239, show WE2 in at least one type of fitting used for the analysis.

For HD 16160, there are data for only two cycles with little variations in the cycle duration and amplitude and the fitting of the data with the analytical profile is also poor. Thus we may expect that when high-quality data are available, this star may show a WE2 relation. The same expectation can be held for HD 155886 because this star also has only two usable cycles and both cycles are very noisy. Interestingly, in HD 161239 the first cycle is very different from the rest; it is the strongest cycle and the activity level, even during the cycle minimum, is relatively high; see Figure 1. This produces an unexpectedly slow rise rate in the first cycle and breaks the WE2 relation. If we do not consider the first cycle, then the star beautifully shows WE2 (the linear Spearman correlation is 0.8 for quasi-Planck fitted data and 0.2 for skewed-Gaussian fitting). HD 81809 is a peculiar star. In the available observation period, it has four excellent cycles and the quality of the data is fairly good as is evident with good fittings with the analytical profiles (small $\chi^2_{\rm red}$). Still, the star does not show Waldmeier Effect. This possibly gives a hint that the periodicity of the magnetic cycle in HD 81809 is caused by a different mechanism. Coincidently, HD 81809 is an unresolved binary system and the cyclic magnetic activity is possibly caused by the A component which is a subgiant (with a rotation period of about 40 days and an effective temperature of 5757 K; Egeland 2018). It could be that this slowly rotating subgiant possesses the so-called antisolar differential rotation (Harutyunyan et al. 2016) and consequently, the dynamo mechanism could be fundamentally different from that in the other solar-like stars (Karak et al. 2015; Karak et al. 2019). Incidentally, the possibility of the existence of antisolar differential rotation in slowly rotating stars and the cyclic dynamos in those stars are highlighted in recent observational and theoretical works (Karak et al. 2015; Brandenburg & Giampapa 2018; Warnecke 2018; Karak et al. 2019; Viviani et al. 2019). Clearly, further research is needed to identify the exact dynamo mechanism causing the excellent cycles in HD 81809 and why the Waldmeier Effect is broken in this star.

In contrast to WE2, WE1 is observed to hold only in a small number of stars (5 out of 21, for the quasi-Planck fitting). For the Sun, we already know that the WE2 is a robust feature of the solar cycle and it exists in all the proxies of the solar cycle, while the WE1 correlation is very poor and sensitive to the data quality (Dikpati et al. 2008; Karak & Choudhuri 2011). Our analysis of the chromospheric activity of the Sun also confirms that the WE1 correlation is weaker than the WE2. Thus with our limited data sets for the Sun-like stars, and the existence of a strong correlation between the rise rate and peak S-index (WE2), confirms that other Sun-like stars studied in this paper show the Waldmeier Effect.

The Waldmeier Effect is a very distinctive and stringent feature of the solar cycle which has implication in predicting the activity level of the following cycle (Cameron & Schüssler 2007; Kane 2008; Cameron & Schüssler 2016; Mandal et al. 2017). Explaining this feature is a challenge to the solar dynamo models. However, a correct dynamo model for the solar cycle must explain this special feature (Karak & Choudhuri 2011; Pipin & Kosovichev 2011; Passos & Charbonneau 2014; Mandal et al. 2017). Previously, using 25 yr records of Ca II HK emission fluxes of solar-type stars, Soon et al. (1994) showed a similar type of inverse relationship between the amplitude of activity and the cycle length both for the solar cycles and the ensemble of solar-type stars. This result and the existence of the Waldmeier Effect in other Sun-like stars, as found in the present study, suggest that the same mechanism is responsible for producing magnetic activity cycles in the Sun and other Sun-like G–K stars. Hence, the dynamo models which are successful in explaining the features of the solar cycle can be extended to other Sun-like stars.

It is also worth considering the converse implication; that is, if the Sun and Sun-like stars operate under the same dynamo mechanism, then observational constraints obtained for the stars are also applicable to the Sun. In particular, it has been observed from stellar data that the cycle period increases along with the rotation period (Saar & Brandenburg 1999; Böhm-Vitense 2007) along two branches separated by their activity level and rotation period. More recent reanalyses of the MWO HK Project data have called into question whether such a trend exists for the so-called "active" branch, stars with $\log(R'_{\rm HK}) \gtrsim -4.75$ and semi-empirical Rossby number $\lesssim 1.5$ (Boro Saikia et al. 2018; Olspert et al. 2018). The other, "inactive" branch, however, remains robust in these same studies, and more importantly this cycle branch covers the solar activity-Rossby parameter regime. Both Babcock–Leighton flux transport dynamos (Jouve et al. 2010; Karak et al. 2014) and recent global MHD simulations (Strugarek et al. 2017, 2018) are unable to reproduce this observed cycle period trend (however, see Hazra et al. 2019, who find some correct trends in a pumping-dominated dynamo model). By necessity, our study included only targets with high-quality cycles, which are the same set of stars comprising the inactive branch. By finding the WE operating in these stars, it appears more likely that they are operating the same dynamo mechanism as the Sun, and therefore viable models for the solar cycle should produce an increasing cycle period with an increasing rotation period. This indirect inference suggests that a significant revision in the current dynamo models is required.

We thank Bibhuti Jha and Prasun Dutta for discussions on the data analysis. We further thank the anonymous referee for a careful review and for providing comments. S.G. thanks IIT (BHU) for providing a one-month visit in the initial phase of the project. B.B.K. sincerely thanks SERB/DST for providing a research grant through the Ramanujan Fellowship (project no SB/S2/RJN-017/2018). R.E. was supported by the NCAR Advanced Study Program Postdoctoral Fellowship. The National Center for Atmospheric Research is sponsored by the National Science Foundation.

Appendix
Supplementary Material

This appendix contains supplementary material in the form of tables. The correlation plots and other results can be derived using these data. Tables 3 and 4 contain the fit parameter values for usable cycles and unusable cycles. The fitted curves are

Table 3
List of Fit Parameters for Usable Cycles of the Stars

HD	Cycle #	t_{start}	Quasi-Planck Fit					Skewed-Gaussian Fit					
			a	b	c	t_0	χ^2_{red}	A	B	α	t_m	f_{min}	χ^2_{red}
3651	1	1973.077	−0.00003	21.96642	1.05552	1996.256	15.7	0.03397	2.52670	0.06877	1977.213	0.16074	14.3
	2	1986.891	0.00005	18.42781	1.06091	1979.013	10.0	0.01864	2.26416	0.04595	1994.014	0.16042	8.1
4628	1	1972.138	0.00037	13.55695	−3.30787	1956.948	8.0	0.05232	1.88710	−0.00608	1976.500	0.19686	6.7
	2	1980.805	0.00068	9.06178	0.75710	1974.630	24.4	0.07622	1.64646	0.04085	1984.039	0.19581	15.2
	3	1988.888	0.00049	9.46364	1.03405	1985.272	20.2	0.06302	1.76819	0.01515	1993.597	0.19657	9.3
10476	1	1971.208	0.00017	13.61922	0.67148	1961.034	13.0	0.04810	1.84349	0.01893	1975.644	0.17655	9.4
	2	1981.708	0.00015	14.02285	0.76646	1971.242	21.7	0.04520	1.71951	0.08420	1985.423	0.17267	10.9
	3	1992.274	−0.00019	11.91185	1.05735	2007.279	11.8	0.02371	−1.88174	0.01890	1996.973	0.17389	11.0
16160	1	1977.674	0.00019	13.93008	0.60479	1967.328	17.5	0.05286	2.36702	−0.02248	1982.956	0.20142	16.1
	2	1988.674	0.00019	13.16737	1.03675	1984.667	19.5	0.06283	−3.39093	0.03947	1995.942	0.19624	19.1
20630	1	1977.260	0.00136	7.94665	0.83796	1971.787	9.0	0.07114	1.20693	0.24111	1979.557	0.30363	8.4
	2	1982.093	0.00036	12.33989	0.78578	1971.620	9.2	0.02087	−0.73085	−0.06690	1984.701	0.34015	8.2
	3	1987.593	0.00031	13.20755	0.71826	1976.531	13.5	0.04495	1.28795	0.08658	1990.403	0.32820	11.2
26965	1	1974.350	0.00011	15.62085	0.81033	1962.197	9.1	16.55227	74.08259	0.02908	1978.322	−16.34062	9.1
	2	1984.434	0.00026	11.74674	0.81468	1976.605	8.9	0.12171	4.35422	0.03059	1988.659	0.10445	8.4
	3	1994.017	0.00032	10.38231	1.04316	1990.593	8.8	0.05403	−3.01383	−0.00346	1999.836	0.16298	9.0
32147	1	1976.927	0.00029	12.59847	0.77504	1967.146	24.3	0.26280	4.66508	0.09866	1979.777	0.04906	21.5
	2	1986.260	0.00036	11.13495	1.03585	1983.393	17.7	0.07866	2.95511	0.03546	1993.002	0.22544	16.6
81809	1	1972.440	0.00016	12.66994	0.85374	1963.370	9.1	0.06014	3.73925	0.07183	1975.907	0.11997	8.7
	2	1980.402	0.00011	14.85605	0.80285	1968.688	10.3	0.03604	2.45462	0.10103	1983.514	0.14879	7.7
	3	1989.152	0.00025	11.15987	0.79085	1980.370	6.5	0.04123	2.50524	0.05027	1991.952	0.14185	6.3
	4	1995.652	0.00018	11.83466	1.05833	1990.811	12.1	0.02616	1.48407	−0.13072	2001.061	0.16082	11.1
103095	1	1974.826	0.00037	10.19001	0.79966	1967.278	9.0	0.03542	1.36056	0.06468	1977.521	0.17296	7.7
	2	1981.409	−0.00021	12.63704	0.44887	1999.699	9.0	0.03368	2.03049	−0.01620	1985.168	0.16457	8.5
	3	1988.909	0.00026	11.15162	0.84375	1980.663	6.9	0.03869	2.20636	0.14569	1991.435	0.15881	5.9
	4	1995.492	−0.00030	10.93660	0.75811	2011.034	11.1	0.02731	1.28343	−0.04186	1999.482	0.17863	9.5
115404	1	1976.588	0.00010	22.58563	0.72117	1956.311	23.0	0.22537	5.22062	0.06002	1980.333	0.34573	22.4
	2	1988.588	0.00028	14.96163	0.94085	1978.375	31.3	282.67	205.69	0.02673	1992.821	−282.14	31.2
149661	1	1970.269	0.01221	3.81203	1.03289	1969.268	13.9	0.15751	1.04511	−0.19775	1972.905	0.26208	8.1
	2	1974.220	0.00229	6.62061	0.85257	1968.886	7.8	75.00468	52.97827	0.07636	1975.594	−74.64756	7.9
	3	1977.769	−0.00169	7.01593	1.01273	1986.771	20.9	0.04939	1.47420	−0.15638	1980.582	0.29442	20.7
	4	1982.602	0.00396	5.14714	1.05998	1980.400	25.1	0.03914	−0.75822	0.96105	1983.918	0.29514	23.7
	5	1986.352	0.00111	8.54298	0.86251	1980.437	26.1	133.38	83.86106	0.12729	1988.474	−133.01	22.5
	6	1992.769	−0.00056	10.54707	0.76645	2007.466	22.8	0.04965	−0.44305	−0.47344	1996.829	0.31828	17.8
	7	1998.102	0.00584	4.88098	1.00684	1996.073	18.5	276.26	81.97349	−0.00568	2000.666	−275.86	18.4
152391	1	1973.467	−0.00019	17.06988	0.25778	1999.924	23.4	0.07811	−1.91092	0.04456	1979.719	0.34722	22.6
	2	1984.634	0.00024	14.61202	0.94103	1975.983	22.0	316.32	243.45347	0.01403	1990.243	−315.90	21.9
	3	1994.467	0.00030	13.80294	0.81915	1983.537	46.7	0.07751	−0.81094	0.52461	1996.366	0.35840	31.4
155885	1	1968.515	−0.00049	−11.68000	0.81894	1983.157	15.8	0.03299	0.83394	0.13242	1970.985	0.38463	14.7
	2	1973.598	−0.00075	10.12397	0.83278	1987.052	19.1	34.89182	45.08485	−0.17104	1977.030	−34.47625	18.4
	3	1979.265	0.00084	10.03315	0.67185	1970.014	30.4	0.09207	0.73580	0.27387	1981.179	0.35220	20.1
	6	1995.531	0.00290	6.25400	1.04317	1993.654	33.8	0.10820	0.54075	0.24093	1999.087	0.37812	20.4
155886	1	1968.515	0.00146	7.88908	1.05315	1965.385	19.9	0.08489	0.86324	−0.27408	1972.666	0.38021	13.6
	4	1989.181	1.94477	7.53534	−43424.73	1970.264	28.4	−0.20321	−15.47080	0.16180	1999.423	0.43289	29.2
156026	1	1969.237	2.65535	22.31880	−1184502.4	1902.567	60.4	0.25095	3.42172	−0.05961	1980.496	0.66815	58.4
	2	1986.404	0.00084	11.31426	1.05650	1981.170	108.5	261.26	150.01	−0.07238	1991.608	−260.51	109.3
160346	1	1968.657	−0.02475	−9.11479	−425.93	1992.820	15.9	596.92	171.15	0.05111	1972.061	−596.55	14.9
	2	1976.240	0.00062	10.08616	0.70288	1968.566	31.9	−0.07281	47.46115	0.10467	1989.547	0.32746	19.1
	3	1983.823	0.00078	9.13790	0.74947	1976.597	27.3	0.16106	1.99316	0.21495	1985.622	0.16077	14.9
	4	1990.957	0.00280	5.89130	1.02220	1988.825	25.4	0.10065	0.88474	0.23066	1993.598	0.26608	14.1
161239	1	1968.207	0.00004	17.87804	1.06062	1961.118	6.9	0.01522	2.18507	−0.11828	1978.408	0.13185	6.6
	2	1982.374	0.00019	11.52722	0.54792	1971.630	10.0	0.01128	−0.90487	0.00436	1984.579	0.13176	9.3
	3	1987.540	0.00116	5.83240	1.06613	1985.029	7.0	0.01230	0.62130	0.53831	1989.209	0.13219	6.5
	4	1992.207	0.00009	14.18839	0.80967	1979.752	6.1	0.01278	2.08953	0.04462	1994.462	0.12517	6.1
	5	1997.374	0.00093	6.21154	1.06954	1994.774	8.2	0.01101	0.48922	−0.01211	1999.959	0.13149	7.7
166620	1	1973.907	−0.00006	−18.15521	1.03682	1995.824	23.2	0.05913	−3.64608	0.02849	1979.446	0.16325	18.2
	2	1990.990	0.00005	19.42901	0.78151	1975.706	21.3	0.02689	−1.31451	0.00040	1995.684	0.17729	16.3
201091	1	1969.587	0.01023	9.26666	−34.92482	1956.381	32.9	0.23855	1.32241	0.05963	1973.026	0.58765	27.0
	2	1977.003	0.00104	10.81097	0.81174	1969.221	26.9	−0.22431	37.98379	0.07924	1994.379	0.67393	30.1
	3	1985.087	0.00277	7.93770	0.73027	1980.048	30.8	0.21634	1.98884	0.09979	1988.300	0.49238	30.2
	4	1991.587	3.32037	8.67855	−70877.1	1968.643	24.3	0.50460	−2.93363	−0.08084	1995.371	0.25069	24.1
201092	1	1967.000	0.00889	6.10606	0.80022	1962.519	28.4	556.05	70.15428	0.11064	1968.792	−554.98	28.1
	2	1971.760	−0.00118	12.23483	0.81287	1991.300	65.7	571.56	76.11615	−0.35400	1980.523	−570.44	43.3

Table 3
(Continued)

HD	Cycle #	t_{start}	Quasi-Planck Fit					Skewed-Gaussian Fit					
			a	b	c	t_0	χ^2_{red}	A	B	α	t_m	f_{min}	χ^2_{red}
	5	1997.343	0.00655	6.72303	0.84075	1993.362	49.4	0.32077	−0.95785	0.59137	1999.381	0.78356	36.2
219834B	1	1968.849	0.00019	13.15917	0.75811	1958.099	16.8	0.03996	1.54044	0.09407	1971.896	0.19152	13.5
	2	1977.015	0.00031	10.52077	1.05078	1973.266	52.3	0.05264	2.12248	−0.00475	1982.494	0.17502	48.3
	3	1988.265	0.00025	11.80385	0.79634	1979.495	64.1	0.06813	1.81362	0.15120	1990.869	0.16159	37.5
	4	1997.182	0.00727	7.85046	−58.37132	1985.728	24.8	0.07179	1.38579	0.24365	2000.202	0.18730	14.6

Table 4
List of Fit Parameters for Unusable Cycles

HD	Cycle #	t_{start}	Quasi-Planck Fit					Skewed-Gaussian Fit					
			a	b	c	t_0	χ^2_{red}	A	B	α	t_m	f_{min}	χ^2_{red}
3651	0	1967.808	0.00008	14.73875	1.11571	1960.119	4.1	0.03167	0.67457	0.90677	1967.530	0.15995	4.1
4628	0	1967.805	0.00029	12.65300	0.28500	1952.529	10.5	0.03987	11.70434	−0.24340	1967.233	0.21260	6.8
	4	1998.870	0.00031	11.00919	1.04188	1994.962	11.2	0.03843	2.59672	0.10718	2003.165	0.20019	11.2
10476	0	1967.624	184.34	239.29	220329.3	696.276	7.2	34.03461	9.20649	2.06801	1967.805	−33.81592	5.8
16160	0	1968.841	−2.08536	−86.55002	−3203538.8	2043.742	11.7	−0.10334	−4.51996	−0.02049	1977.208	0.30135	11.1
20630	0	1968.843	0.00044	11.34389	1.09690	1962.617	14.9	0.06800	5.55820	−0.12169	1971.215	0.34104	14.9
	4	1994.800	0.00004	26.33570	0.89218	1973.889	34.7	0.06921	0.55279	−1.00383	2002.515	0.34751	37.3
26965	0	1968.934	−0.00055	4305.5	−592.72	2032.142	15.6	0.04155	2.26920	−0.38731	1969.508	0.18979	5.9
32147	0	1968.843	0.00033	13.10860	0.54002	1955.226	27.5	0.36062	2.64644	0.24537	1970.177	0.01928	12.6
	3	1998.677	0.00785	3525.9	−824.45	1969.406	19.2	0.11311	0.91264	−0.08602	2002.682	0.25432	8.3
81809	0	1967.068	−0.24283	135.91	−225724.3	2024.127	4.6	0.53697	3.96863	0.38283	1967.168	−0.33681	4.4
103095	0	1969.326	0.00016	13.69542	0.68319	1955.239	6.9	14.81514	33.93372	0.21716	1970.436	−14.60824	6.2
155885	4	1985.456	0.00041	11.99483	0.87560	1976.661	24.1	0.02134	0.67884	0.68844	1988.540	0.35696	34.2
	5	1992.200	0.00166	7.68229	0.79647	1985.495	25.6	65.72575	36.34042	0.43686	1993.110	−65.32469	24.7
155886	2	1975.848	0.00056	11.12578	0.72436	1965.695	11.0	45.88451	39.58132	0.25605	1977.346	−45.48709	10.7
	3	1981.265	0.00012	18.00152	0.81553	1965.094	35.8	0.06358	0.17859	2.82572	1982.452	0.33595	17.9
	5	1995.181	0.00003	30.59362	0.77630	1962.898	26.8	0.04361	0.21721	−0.41962	1996.628	0.37549	15.9
156026	3	1995.280	0.00002	48.45743	0.96648	1968.338	25.7	−0.12203	−176.97	0.04332	2024.654	0.90965	25.6
160346	5	1997.407	0.00028	12.73184	0.90492	1989.259	12.3	−0.05695	1.20040	−0.15781	1997.560	0.31172	11.0
166620	0	1967.490	0.00014	12.75945	1.10908	1961.428	5.7	0.00851	1.79696	−0.50082	1970.188	0.18084	5.6
201092	3	1982.343	0.00103	11.44072	1.08425	1976.439	46.1	0.09411	−0.22063	1.13625	1985.064	0.95599	46.1
	4	1987.593	0.00044	16.39994	0.77715	1973.197	38.4	0.58815	4.87670	0.07907	1990.070	0.44106	37.7

Note. Cycle #0 refers to the initial partial cycle.

Table 5
Peak *S*-index, Rise Times, and Rates of All Usable Cycles in Each Star

HD	Cycle #	Quasi-Planck Fit			Skewed-Gaussian Fit		
		Peak	*r*Rate	*r*Time	Peak	*r*Rate	*r*Time
3651	1	0.18337	0.00193	4.08333	0.19471	0.01116	1.91667
	2	0.17585	0.00247	3.83333	0.17905	0.00026	2.08333
4628	1	0.24400	0.01588	2.25000	0.24917	0.01348	2.08333
	2	0.26172	0.02163	1.66667	0.27203	0.03091	1.50000
	3	0.24875	0.01791	2.41667	0.25958	0.01308	1.83333
10476	1	0.21654	0.01350	2.33333	0.22465	0.01241	2.16667
	2	0.20730	0.01069	2.08333	0.21786	0.01813	1.41667
	3	0.19456	0.00826	2.33333	0.19759	0.00531	2.00000
16160	1	0.24944	0.01710	2.25000	0.25428	0.00967	3.58333
	2	0.25672	0.01113	3.58333	0.25907	0.00648	2.75000
20630	1	0.36284	0.02250	1.25000	0.37473	0.04399	0.75000
	2	0.35601	0.00769	0.75000	0.36101	0.01294	1.58333
	3	0.36306	0.01197	1.16667	0.37314	0.02452	1.83333
26965	1	0.21072	0.00774	1.83333	0.21165	0.00897	1.75000
	2	0.22545	0.01620	1.91667	0.22616	0.01746	1.91667
	3	0.21582	0.01123	2.50000	0.21701	0.00920	2.83333
32147	1	0.30300	0.01330	1.41667	0.31186	0.02212	1.25000
	2	0.29910	0.01324	4.50000	0.30410	0.00876	2.58333
81809	1	0.17986	0.00888	1.75000	0.18012	0.01053	1.50000
	2	0.18189	0.00650	1.75000	0.18483	0.01131	1.66667
	3	0.18231	0.00704	1.33333	0.18307	0.00833	1.41667
	4	0.18238	0.00550	2.66667	0.18698	0.00310	3.91667
103095	1	0.20525	0.01074	1.50000	0.20838	0.01698	1.75000
	2	0.19617	0.00879	1.75000	0.19825	0.00922	2.25000
	3	0.19601	0.00886	1.50000	0.19750	0.01035	1.08333
	4	0.20207	0.01112	1.75000	0.20594	0.00705	2.91667
115404	1	0.56161	0.00977	0.66667	0.57110	0.02425	1.50000
	2	0.52006	0.02029	1.91667	0.52050	0.02214	1.83333
149661	1	0.40591	0.05149	1.25000	0.41952	0.05803	1.83333
	2	0.35677	0.02584	0.33333	0.35710	0.02737	0.33333
	3	0.34502	0.01548	1.16667	0.34380	0.01250	1.25000
	4	0.33207	0.01449	1.00000	0.33428	0.03913	0.66667
	5	0.37405	0.02100	1.25000	0.37266	0.01355	0.91667
	6	0.34182	0.01714	1.75000	0.36786	0.00247	3.50000
	7	0.39966	0.03977	1.16667	0.39984	0.03958	1.16667
152391	1	0.41087	0.01995	3.00000	0.42532	0.00200	3.91667
	2	0.41707	0.02461	2.50000	0.41659	0.02560	1.66667
	3	0.40970	0.01370	1.25000	0.43589	0.05929	1.00000
155885	1	0.41012	0.00824	0.33333	0.41760	0.02513	1.66667
	2	0.41478	0.01633	1.08333	0.41556	0.01378	1.75000
	3	0.41979	0.00201	1.75000	0.44428	0.05823	0.66667
	6	0.42966	0.03844	1.75000	0.48630	0.00001	2.45833
155886	1	0.43646	0.02399	1.58333	0.46509	0.01321	3.08333
	4	0.43613	0.04431	1.91667	0.43289	0.04327	1.58333
156026	1	0.91094	0.02916	6.00000	0.91910	0.01062	7.25000
	2	0.74860	0.02655	2.50000	0.74832	0.02086	2.50000
160346	1	0.36610	0.04774	1.58333	0.36466	0.05019	1.41667
	2	0.31719	0.01900	1.41667	0.32746	0.01845	2.16667
	3	0.30662	0.01231	0.91667	0.32181	0.01240	0.83333
	4	0.34045	0.03788	1.58333	0.36669	0.07513	1.91667
161239	1	0.14510	0.00129	4.33333	0.14706	0.00050	6.08333
	2	0.14098	0.00261	1.08333	0.14304	0.00599	1.08333
	3	0.14238	0.00565	1.16667	0.14449	0.00582	0.41667
	4	0.13780	0.00182	1.00000	0.13795	0.00201	1.00000
	5	0.13834	0.00517	1.25000	0.14251	0.00642	0.58333
166620	1	0.21458	0.00561	1.83333	0.22238	0.01183	2.91667
	2	0.19361	0.00663	2.58333	0.20417	0.00312	3.66667
201091	1	0.78728	0.07623	2.00000	0.82616	0.10021	2.41667
	2	0.69158	0.03955	1.41667	0.67393	0.03894	2.16667
	3	0.70488	0.07721	1.50000	0.70868	0.09043	1.33333
	4	0.75438	0.06348	2.08333	0.75525	0.06386	2.25000
201092	1	1.05982	0.03324	0.75000	1.06719	0.02885	0.75000
	2	1.13756	0.08544	3.25000	1.12020	0.01596	6.75000
	5	1.06192	0.11032	1.33333	1.10408	0.29693	0.41667
219834B	1	0.22465	0.00771	0.91667	0.23147	0.01977	1.83333
	2	0.22145	0.00908	2.50000	0.22766	0.00852	3.58333
	3	0.21575	0.01109	1.66667	0.22971	0.02723	1.08333
	4	0.25346	0.03018	1.75000	0.25908	0.04676	2.16667

defined by Equations (1) and (2). Using the data provided in Tables 3 and 4, the plots in Figure 1 can be reproduced, whereas, the plots in Figures 5 and 6 can be obtained from Table 5.

ORCID iDs

Bidya Binay Karak https://orcid.org/0000-0002-8883-3562
Ricky Egeland https://orcid.org/0000-0002-4996-0753

References

Baliunas, S. L., Donahue, R. A., Soon, W. H., et al. 1995, ApJ, 438, 269
Bertello, L., Pevtsov, A., Tlatov, A., & Singh, J. 2016, SoPh, 291, 2967
Böhm-Vitense, E. 2007, ApJ, 657, 486
Boro Saikia, S., Marvin, C. J., Jeffers, S. V., et al. 2018, A&A, 616, A108
Brandenburg, A., & Giampapa, M. S. 2018, ApJL, 855, L22
Cameron, R., & Schüssler, M. 2007, ApJ, 659, 801
Cameron, R., & Schüssler, M. 2008, ApJ, 685, 1291
Cameron, R. H., & Schüssler, M. 2016, A&A, 591, A46
Charbonneau, P. 2014, ARA&A, 52, 251
Dikpati, M., Gilman, P. A., & de Toma, G. 2008, ApJL, 673, L99
Du, Z. 2011, SoPh, 273, 231
Egeland, R. 2017, PhD thesis, Montana State Univ., Bozeman, Montana, USA, https://scholarworks.montana.edu/xmlui/handle/1/12774
Egeland, R. 2018, ApJ, 866, 80
Egeland, R., Soon, W., Baliunas, S., et al. 2017, ApJ, 835, 25
Gilman, P. A. 1983, ApJS, 53, 243
Halm, J. 1901, AN, 156, 33
Halm, J. 1902, AnEdi, 1, 71
Harutyunyan, G., Strassmeier, K. G., Künstler, A., Carroll, T. A., & Weber, M. 2016, A&A, 592, A117
Hathaway, D. H., Wilson, R. M., & Reichmann, E. J. 1994, SoPh, 151, 177
Hazra, G., Jiang, J., Karak, B., & Kitchatinov, L. 2019, ApJ, 884, 35
Jouve, L., Brown, B. P., & Brun, A. S. 2010, A&A, 509, A32
Kane, R. P. 2008, JASTP, 70, 1533
Karak, B. B., & Choudhuri, A. R. 2011, MNRAS, 410, 1503
Karak, B. B., Käpylä, P. J., Käpylä, M. J., et al. 2015, A&A, 576, A26
Karak, B. B., Kitchatinov, L. L., & Choudhuri, A. R. 2014, ApJ, 791, 59
Karak, B. B., Tomar, A., & Vashishth, V. 2019, MNRAS, arXiv:1910.11893
Lean, J. L., & Brueckner, G. E. 1989, ApJ, 337, 568
Leighton, R. B. 1959, ApJ, 130, 366
Mandal, S., Karak, B. B., & Banerjee, D. 2017, ApJ, 851, 70
Moffatt, H. K. 1978, Magnetic Field Generation in Electrically Conducting Fluids (Cambridge: Cambridge Univ. Press)
Moré, J. J. 1978, Numerical Analysis (Berlin: Springer)
Noyes, R. W., Hartmann, L. W., Baliunas, S. L., Duncan, D. K., & Vaughan, A. H. 1984, ApJ, 279, 763
Oláh, K., Kővári, Z., Petrovay, K., et al. 2016, A&A, 590, A133
Olspert, N., Lehtinen, J. J., Käpylä, M. J., Pelt, J., & Grigorievskiy, A. 2018, A&A, 619, A6
Ossendrijver, M. 2003, A&ARv, 11, 287
Parker, E. N. 1955, ApJ, 122, 293
Passos, D., & Charbonneau, P. 2014, A&A, 568, A113
Pipin, V. V., & Kosovichev, A. G. 2011, ApJ, 741, 1
Ramesh, K. B., & Lakshmi, N. B. 2012, SoPh, 276, 395
Saar, S. H., & Brandenburg, A. 1999, ApJ, 524, 295
Schrijver, C. J., Dobson, A. K., & Radick, R. R. 1992, A&A, 258, 432

Schröder, K. P., Mittag, M., Hempelmann, A., González-Pérez, J. N., & Schmitt, J. H. M. M. 2013, A&A, 554, A50
Skumanich, A., Smythe, C., & Frazier, E. N. 1975, ApJ, 200, 747
Soon, W. H., Baliunas, S. L., & Zhang, Q. 1993, ApJL, 414, L33
Soon, W. H., Baliunas, S. L., & Zhang, Q. 1994, SoPh, 154, 385
Strugarek, A., Beaudoin, P., Charbonneau, P., & Brun, A. S. 2018, ApJ, 863, 35
Strugarek, A., Beaudoin, P., Charbonneau, P., Brun, A. S., & do Nascimento, J.-D. 2017, Sci, 357, 185
Viviani, M., Käpylä, M. J., Warnecke, J., Käpylä, P. J., & Rheinhardt, M. 2019, MPS, ReSoLVE/Aalto, and IAG, arXiv:1902.04019
Waldmeier, M. 1935, MiZur, 14, 105
Warnecke, J. 2018, A&A, 616, A72